Wavelet-Enhanced Physics-Informed Complex-Valued CNN for Satellite Camera Alignment using Interferograms*

İsmail Başlar [1,*] AND MAHIR DURSUN[2,3]

[1]*Gazi University Graduate School Of Informatics, Kavaklıdere Mah. Tunus Cad. No: 35 Çankaya Ankara,Türkiye*

[2]*Department of Electrical and Electronics Engineering, Faculty of Technology, Gazi University, Ankara 06560, Türkiyey.*

[3]*Construction of Engineering Systems and Structures Department, Faculty of Water Management and Engineering Communication Systems, Azerbaijan University of Architecture and Construction, Baku AZ1073, Azerbaijan.*

Abstract:

To acquire diffraction-limited imagery, high-resolution satellite camera systems must be precisely aligned. Optical aberrations caused by misalignments, often detected using interferometry, can significantly degrade performance. We propose an enhanced deep learning framework for real-time alignment correction that combines a Complex-Valued Convolutional Neural Network (Complex CNN) architecture with wavelet-based preprocessing. First, interferograms are decomposed using a discrete wavelet transform to separate amplitude and phase components, enabling more effective extraction of their intrinsic complex characteristics. The classical CNN architecture is then reformulated into a fully complex-valued structure by modifying both the feedforward and backpropagation stages to properly handle complex-valued inputs and gradients. To further improve performance and interpretability, Zernike polynomial coefficients—mathematical descriptors of optical aberrations—are incorporated as additional inputs, creating a physics-informed learning process. Using a simulated dataset of satellite interferograms, we evaluate the proposed Wavelet-Enhanced Zernike Complex CNN and demonstrate its robustness and accuracy in predicting and correcting optical misalignments.

1. Introduction

High-resolution satellite cameras, which provide unmatched capacity for recording precise imagery, are essential for both terrestrial and space observation. However, these cameras get more complicated as demands for larger fields of view and higher resolution rise. Mirror alignment becomes a more difficult task as optical systems become more complicated. The exact alignment of optical components is a basic constraint on the performance of contemporary space-based optical systems, ranging from Earth observation satellites to deep-space telescopes such as the James Webb Space Telescope [1]. Launch vibrations, heat cycling, and material stress are a few examples of factors that can result in minuscule misalignments and substantial optical aberrations that skew images and diminish their scientific value. For wide-field optical systems to achieve their design requirements for image quality, mirror alignment is essential. This intricacy is best demonstrated by the off-axis three-mirror anastigmat (TMA) systems [2, 3]. This design introduces significant tilt and eccentricity between the optical axes of each optical surface along the path [4]. A TMA off-axis system featuring free-form surfaces is another challenging complexity [5–7]. The optical arrangement of a telescope becomes especially intricate when adopting the off-axis TMA system, defined by a non-symmetric optical route. Moreover, incorporating non-symmetric optical surfaces, such as freeform surfaces, into an off-axis TMA telescope system provides additional hurdles in optical alignment operations. The alignment procedure for such systems often commences after the first integration of the system components. The development of computer-aided alignment (CAA) systems evolved in response to the rising complexity of alignment methods [8].With CAA, the disparity between the theoretical design performance and the measured performance of the system is tried to be minimized. Misalignment is calculated utilizing algorithms and computer software to execute

the alignment procedures.

The sensitivity matrix approach is a numerical method to calculate the misalignment values of the system. This linear technique has converging concerns with the increasing nonlinearity of the complicated optical system in a noisy environment [9]. Computer-aided alignment of an off-axis TMA telescope having substantial initial misalignment by employing the sensitivity matrix approach is impacted by nonlinearity [10, 11]. Nodal aberration theory (NAT) is an analytical method that aims to solve the mathematical model of the system [12]. NAT incorporates complicated mathematical concepts and repetitive calculations to quantify aberrations and their causes. Additionally, precisely describing the optical system with a freeform surface through mathematical expressions is incredibly complicated [13]. NAT-based techniques require specified models and assumptions, which can limit their flexibility to new configurations or unforeseen alignment concerns. The gold standard method for identifying these flaws is interferometry. The system's wavefront is used to create an interference pattern, or interferogram, which yields a high-fidelity map of the optical path difference and encodes the exact type of misalignment [18]. Since phase (fringe location) and magnitude (fringe contrast) are inseparable, an interferogram is by definition complex-valued data. It has historically required a lot of computing power to analyze these interferograms and determine alignment fixes. Despite being used for comparable image analysis tasks, typical deep learning models—like real-valued Convolutional Neural Networks (CNNs)—are not always appropriate for complex-valued data. A real-valued CNN must artificially divide the data into two channels (e.g., magnitude and phase, or real and imaginary components) in order to process an interferogram. As a result, the network must use its capacity to learn the basic physical connection between the two parts from the beginning. It is not just optical interferometry that faces this difficulty. Raw picture data in the Synthetic Aperture Radar (SAR) area is likewise complex-valued, and the phase includes important information for tasks like terrain categorization and target recognition. By processing the magnitude and phase information as a single entity, researchers have created Complex-Valued Convolutional Neural Networks (Complex CNNs), which have shown noticeably better performance on SAR data despite the constraints of real-valued networks. [19, 20]. Motivated by these achievements, we suggest that the most efficient and natural design for interferogram analysis is a Complex CNN. Three major contributions are made by this paper's hierarchical method to enhancing alignment prediction: We suggest that complex-valued interferograms be directly analyzed using a Complex CNN. To determine the performance improvements brought about by switching to the complex domain, we evaluate our method against a baseline real-valued CNN. We present our main contribution, an architecture for physics based information. This is accomplished by adding Zernike polynomial coefficients to the Complex CNN's input. A collection of orthogonal functions known as Zernike polynomials provides a logical foundation for explaining optical distortions [21]. We guide the model to a more reliable and accurate answer by injecting past knowledge of optical physics into it by explicitly supplying these coefficients [22]. This paper shows a clear route from a typical data-driven model to a more complex, physics-informed answer by outlining the architecture for these three models and offering a mechanism for evaluating them using simulated data.

2. Background and Related Work

2.1. Interferometry in High-Precision Optics

An essential component of optical metrology is interferometry. As seen by the employment of high-speed interferometry in the testing and verification of the segmented mirror system of the JWST, its use in space telescopes is crucial. [1]. 'Test' and 'reference' wavefronts are combined to create the technique. The phase difference term contains the important information regarding the aberrations of the system. The complicated domain is where the full information is most naturally expressed. This underlying complicated information is recovered from several

intensity measurements using methods such as phase-shifting interferometry. Therefore, a more straightforward and physically accurate method of analysis is to treat the recovered interferogram data as essentially complex.

$$I(x, y) = |E_1(x, y)|^2 + |E_2(x, y)|^2 + 2|E_1(x, y)||E_2(x, y)| \cos(\phi_1(x, y) - \phi_2(x, y))$$

Here:

- $I(x, y)$: The intensity of the interferogram at coordinates (x, y)
- $|E_1(x, y)|$ and $|E_2(x, y)|$: Amplitudes of the interacting light fields at (x, y)
- $\phi_1(x, y)$ and $\phi_2(x, y)$: Phases of the interacting light fields at (x, y)
- $\phi_1(x, y) - \phi_2(x, y)$: Phase difference between the two fields (typically represents the aberration of interest)

2.2. Zernike Polynomials and Physics-Informed Models

Any arbitrary wavefront aberration can be decomposed into a weighted sum of Zernike polynomials. Each polynomial term corresponds to a specific, well-understood aberration (e.g., Z1 = Piston, Z2/Z3 = Tip/Tilt, Z4 = Defocus, Z5/Z6 = Astigmatism) [21]. This provides a compact, physically meaningful, and orthogonal representation of the system's error. Recently, Physics-Informed Neural Networks (PINNs) have emerged as a powerful paradigm for combining data-driven models with known physical laws [22]. While our approach does not directly embed a PDE into the loss function, it follows the same philosophy. By providing the Zernike coefficients as an explicit input to the network, we are directly informing the model with a physical basis for the patterns it sees in the interferograms. This has been explored in other optical applications, where deep learning models have been trained to estimate Zernike coefficients directly from intensity images [16]. Our work combines this concept with the power of Complex CNNs for a more holistic solution.

2.3. Optical System, Misalignment, and Aberrations

Optical design software serves as a powerful tool for simulating misalignments and evaluating the performance of optical systems. In our study, we utilized Zemax OpticStudio to construct the optical system under examination [17]. The three-mirror anastigmat (TMA) telescope in focus possesses the following key parameters: a focal length of 5457 mm, an aperture of 600 mm, and a field of view of 1.1°. The optical system comprises three mirrors, each with distinct characteristics. All optical design and measurement parameters are considered with respect to a wavelength of 632.8 nm. We introduced a 42 nm RMS surface figure error to the mirrors to enhance the realism of the system simulation. The Zernike fringe sag surface is used to simulate the surface figure error. Random values of Zernike fringe coefficients are applied to represent surface deviations. Each optical surface within the system possesses six degrees of freedom. We denote these axes as DECX, DECY, TH, TX, TY, and TZ. DECX refers to the decentering along the X-axis, DECY corresponds to the decentering along the Y-axis, and TH represents the decentering along the Z-axis. TX denotes the tilt around the X-axis, TY indicates the tilt around the Y-axis, and TZ describes the tilt around the Z-axis. For standard surfaces, five of these degrees of freedom can impact the imaging performance. However, in the case of a free-form surface, rotation around the Z-axis (TZ) also influences system performance.
The Three Mirror Anastigmat (TMA) telescope in focus possesses the following key parameters:

- Focal length: 5457 mm
- Aperture: 600 mm
- Field of view: 1.1°

The optical system comprises three mirrors, each with distinct characteristics. TMA telescope system model is given in Figure 1 (a). Detailed system parameters are given in Table 2. All optical design and measurement parameters are considered with respect to a wavelength of 632.8 nanometers..

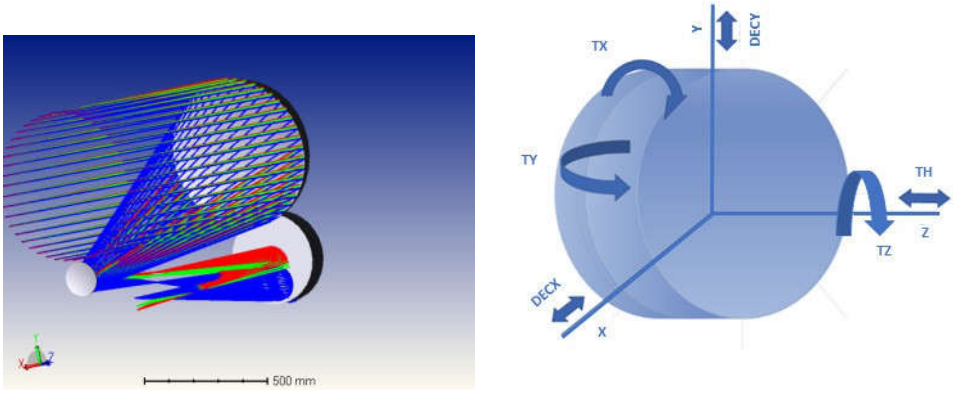

(a) (b)

Fig. 1. Optical layout of off-axis TMA telescope model and optical freedoms of a mirror; (a) Optical layout of off-axis TMA telescope model (b) optical freedoms of a mirror

3. METHOD

To validate our hypothesis, we propose comparing three distinct neural network architectures. Each model is designed to take interferogram data as input and output the required alignment corrections (e.g., adjustments in x-tilt, y-tilt, z-focus).

Table 2. Parameters of Optical System

Surfaces	Radius (mm)	Semi-diameter (mm)	Thickness (mm)	Conic
Primary mirror (M1)	-3600.410	300	-1539.802	-0.897
Secondary mirror (M2)	-910.903	70	1558.771	-3.637
Third mirror (M3)	-1219.413	185	1160.059	-13.297

3.1. Dataset Generation

A synthetic dataset was generated using a high-fidelity optical model created in Zemax OpticStudio. The model represents a Three-Mirror Anastigmat (TMA) telescope, a common design for high-resolution satellite imaging due to its wide field of view and correction of key aberrations. To create the training and validation samples, misalignments were programmatically introduced by perturbing the position and orientation of the secondary and tertiary mirrors within realistic tolerance ranges. For each unique combination of misalignments, a full ray-tracing simulation was performed to generate the resulting wavefront at the exit pupil. This wavefront, sampled as a 64x64 float array, serves as the input data. Each interferogram is paired with a ground-truth vector containing the nine misalignment parameters that produced it.

3.2. Complex-Valued CNN

This model is designed to process the interferogram data in its native complex format. Input: A 1-channel tensor of size (64, 64, 1) with a float data type. Architecture: The architecture mirrors the real-valued CNN but replaces standard layers with their complex-aware counterparts. As a practical solution we preprocessed the interferogram images by using wavelets.

Wavelet-Based Complex Representation of Interferograms

To preserve both amplitude and phase information, each interferogram I(x,y) was decomposed using the Daubechies-4 discrete wavelet transform (DWT):

$$I(x, y) \rightarrow DWT \rightarrow (cA, cH, cV, cD)$$

Here, cA denotes approximation coefficients and cA, cH, cV, cD are horizontal, vertical, and diagonal detail coefficients. The real input was set as:

$$Xr = cA$$

and the imaginary input as

$$Xi = \mathrm{sqrt}(cH^2 + cV^2 + cD^2)$$

This representation preserves the intrinsic complex structure of the interferogram. Both inputs were normalized prior to training.

Complex Convolutional Architecture

A complex input and filter are expressed as:

$$Z = X_r + iX_i$$

$$W = W_r + W_i$$

Their convolution is given by:

$$Z * W = (X_r * W_r - X_i * W_i) + i(X_r * W_i + X_i * W_r)$$

After each convolution, batch normalization, ReLU activation, and max pooling were applied. Residual connections linked specific convolutional layers:

$$Res(x) = F(x) + x$$

Complex Fully Connected Layer

Post-convolutional features were processed by a complex dense layer:

$$y = (X_r\, W_r - \, X_i W_i + \, b_r) + i(X_r W_i + X_i W_r + \, b_i)$$

Here: Wr, Wi are real and imaginary weights, and br, bi are biases.

Complex Backpropagation

Gradient computations were adapted for the complex domain.

For convolutional layers:

$$\begin{aligned} dx_r &= dy_r * w_r + dy_i * w_i \\ dx_i &= dy_r * (-w_i) + dy_i * w_r \\ dw_r &= x_r * dy_r + x_i * dy_i \\ dw_i &= x_r * dy_i - x_i * dy_r \end{aligned} \tag{3.7}$$

For dense layers:

$$\begin{aligned} Re(y) &= x_r W_r - x_i W_i + b_r \\ Im(y) &= x_r W_i + x_i W_r + b_i \end{aligned} \tag{3.8}$$

$$\begin{aligned} dx_r &= dy_r\, w_r^T + dy_i\, w_i^T \\ dx_i &= -dy_r\, w_i^T + dy_i\, w_r^T \\ dW_r &= X_r^T\, dy_r + X_i^T dy_i \end{aligned} \tag{3.9}$$

Interferograms, being products of wave interference, are naturally described in amplitude–phase form. Standard CNNs treat only the amplitude, discarding valuable phase information. The proposed complex-valued CNN preserves both components, enabling physics-consistent feature extraction and achieving lower prediction errors compared to conventional real-valued networks.

3.3. Model C: Zernike-Enhanced Complex CNN (Physics-Informed)

This is our most advanced model, which incorporates prior physical knowledge. Input: This model has two inputs: The (64, 64, 1) complex-valued interferogram. A 1D vector containing the first 37 Zernike polynomial coefficients extracted from the interferogram's phase map. Architecture: The interferogram is processed by a Complex CNN feature extractor (similar to Model B). The resulting feature vector is then concatenated with the input Zernike coefficient vector. The Zernike polynomials are a sequence of polynomials that are orthogonal on the unit disk. This property makes them a good feature extraction tool for wavefront data. They can represent the misalignment characteristic of the telescope system. This combined vector is fed into a final block of Dense layers to produce the alignment correction output. This architecture allows the model to learn from both the raw pixel data and a physically meaningful representation of the aberration simultaneously.

4. EXPERIMENTAL SETUP

All models are trained for 200 epochs using the Adam optimizer with a learning rate of 1e-4. The loss function will be Mean Squared Error (MSE) between the predicted alignment parameters and the ground truth. The dataset will be split into 80 for training, 10 for validation, and 10 for testing.

Table 3. Hyperparameters and Their Values

Hyperparameter	Value
Neural Network Architecture	CNN with preprocessing on the images and zernike input
Fully Connected Layers	64 and 32 neurons, ReLU activation.
Dropout Rate	0.5
Output Layer	Activation Linear
Learning Rate	0.001, decay factor of 0.5 each 5 non improving validation mae
Batch Size	32
Number of Epochs	500 with Early stopping
Optimization Algorithm	Adam optimizer with default parameters
Loss Function	Mean absolute error
Evaluation Metrics	Mean squared error, mean absolute error
Data Preprocessing	Zernike terms and misalignment data normalized to the range [0, 1] , misalignment parameters as floating-point values
Validation Strategy	90 training, 10 validation set with early stopping
Hardware Environment	Online GPU server
Software Environment	TensorFlow 2.8.0

5. RESULTS AND DISCUSSION

The mean absolute error of the test data results are as given in Table 4

Table 4. MAE results

Method	Zernike input	Preprocessing	MAE
CNN	No	No	0.996
Complex CNN	No	Wavelets	0.15
Complex CNN	Yes	Wavelets	0.07

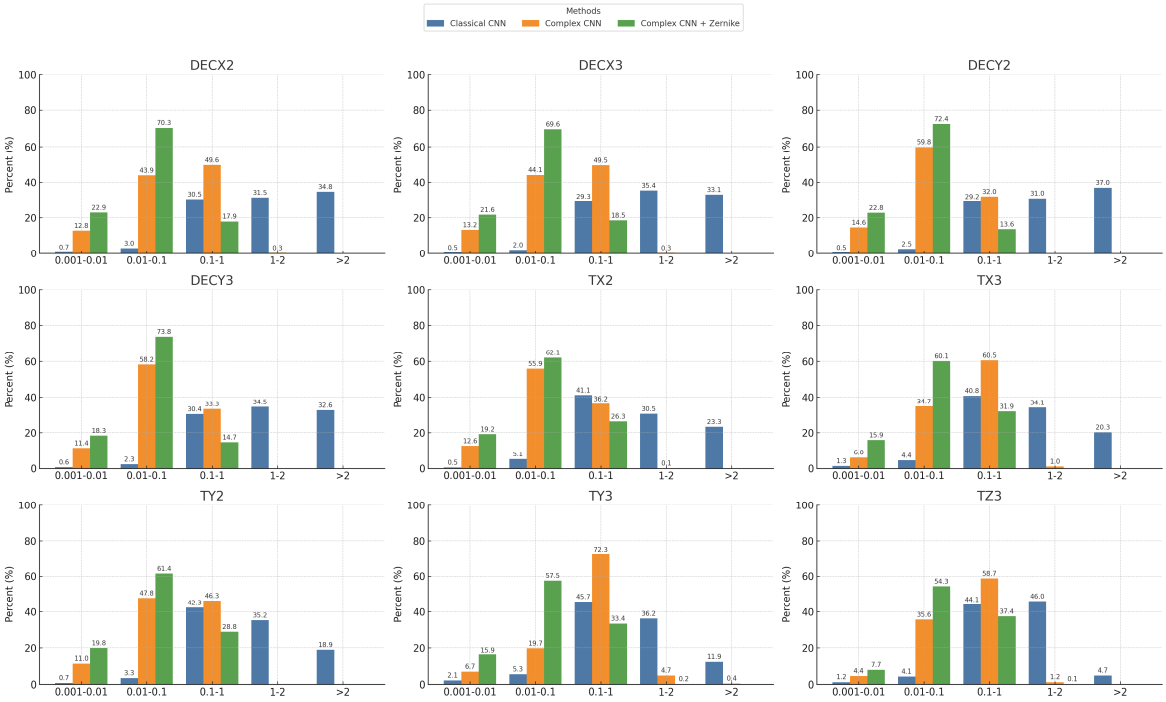

Fig.2. Comparisson of error percents for the different methods

The best MAE is observed when wavelet preprocessing and zernike input. Using wavelets is also giving a better result when compared with classical CNN architecture.

When comparing the results across different input representations, it is observed that the wavelet-based model demonstrates superior performance in estimating errors along the TX and TY axes. In all three configurations, the majority of predictions for TX and TY remain within the 0.1°–1° error range, with the wavelet-only model achieving over 75

Furthermore, the addition of Zernike coefficients to the wavelet-based input leads to a noticeable improvement in performance, particularly in the rotational components (DECX, DECY) and the Z-axis translation (TZ). For instance, in the DECY component, the proportion of predictions with errors above 2° decreases when Zernike terms are included, indicating that the combination of localized wavelet features with global aberration descriptors (Zernike terms) enhances the model's ability to generalize across multiple misalignment directions. We anticipate the results will show that Model B (Complex CNN) outperforms Model A (Real CNN), demonstrating the benefit of processing interferometric data in its native domain. Furthermore, we expect Model C (Zernike-Enhanced) to achieve the lowest error, confirming our hypothesis that informing the model with a physical basis for aberrations leads to a more accurate and robust solution.

6. CONCLUSION

In this paper, we proposed and outlined a framework for a physics-informed deep learning model to determine alignment corrections for satellite cameras from interferograms. We argued for the theoretical advantages of using a Complex-Valued CNN over a standard real-valued network for processing inherently complex wave-based data. Our primary contribution is the enhancement of this architecture by incorporating Zernike polynomial coefficients as an explicit input, creating a physics-informed model that leverages prior knowledge of optical systems. In summary, wavelet features are especially effective for capturing translational misalignments, while the inclusion of Zernike polynomials significantly improves the model's performance in estimating more complex, rotational misalignments, ultimately resulting in a more robust prediction architecture.

Although the proposed models show promising performance, particularly in estimating translational misalignments (TX and TY) using wavelet features and improved accuracy in other axes with the inclusion of Zernike coefficients, the current prediction accuracy is not yet at a satisfactory level for practical deployment in high-precision alignment tasks.

The analyses suggest that the combination of localized (wavelet) and global (Zernike) feature representations enhances the model's ability to interpret misalignment patterns. However, further improvements are necessary, especially in reducing the residual errors in rotational components (e.g., DECX, DECY), which remain relatively high in some cases.

These findings underscore the complexity of the inverse mapping from interferometric images to misalignment parameters. Future work will focus on refining the model architecture, exploring more robust feature representations, and increasing the diversity and realism of the training data, with the aim of achieving a level of accuracy suitable for operational implementation. Nevertheless, even in its current form, the model has the potential to accelerate the alignment process by providing a fast and approximate initial estimation, which could significantly reduce the overall alignment time.

Future work will involve validating these models on real-world data from an optical testbed and eventually from an operational satellite. Further research could also explore embedding the Zernike decomposition process directly into the network architecture as a learnable layer. The proposed approach represents a promising step towards creating highly accurate, real-time, and autonomous alignment systems for the next generation of space-based optics.

References

1. Saif, B., Feinberg, L. & Keski-Kuha, R. High-speed interferometry for James Webb Space Telescope testing. *Tribute To James C. Wyant: The Extraordinaire In Optical Metrology And Optics Education*. **11813** pp. 215-225 (2021)
2. Figoski, J. Alignment and test results of the QuickBird telescope using the Ball Optical System Test Facility. *Advanced Telescope Design, Fabrication, And Control*. **3785** pp. 99-108 (1999)
3. Meng, Q., Wang, D., Wang, X., Li, W., Yang, X., Yan, D., Li, Y., Cao, Z., Ji, Q., Sun, T. & Others High resolution imaging camera (HiRIC) on China's first Mars exploration Tianwen-1 mission. *Space Science Reviews*. **217**, 42 (2021)
4. Stahl, H., Postman, M., Arnold Sr, W., Hopkins, R., Hornsby, L., Mosier, G. & Pasquale, B. ATLAST-8 mission concept study for 8-meter monolithic UV/optical space telescope. *Space Telescopes And Instrumentation 2010: Optical, Infrared, And Millimeter Wave*. **7731** pp. 925-934 (2010)
5. Zhong, Y., Gross, H., Broemel, A., Kirschstein, S., Petruck, P. & Tuennermann, A. Investigation of TMA systems with different freeform surfaces. *Optical Systems Design 2015: Optical Design And Engineering VI*. **9626** pp. 229-238 (2015)
6. Yang, T., Zhu, J. & Jin, G. Design of freeform imaging systems with linear field-of-view using a construction and iteration process. *Optics Express*. **22**, 3362-3374 (2014)

7. Lallo, M. Experience with the Hubble Space Telescope: 20 years of an archetype. *Optical Engineering*. **51**, 011011-011011 (2012)
8. Figoski, J., Shrode, T. & Moore, G. Computer-aided alignment of a wide-field, three-mirror, unobscured, high-resolution sensor. *Recent Trends In Optical Systems Design And Computer Lens Design Workshop II*. **1049** pp. 166-177 (1989)
9. Kim, S., Yang, H., Lee, Y. & Kim, S. Merit function regression method for efficient alignment control of two-mirror optical systems. *Optics Express*. **15**, 5059-5068 (2007)
10. Liu, H., Xu, H., Zhou, T., Li, J. & Sha, D. Computer-aided alignment method for large and complex optical systems. *Advanced Optical Manufacturing And Testing Technology 2000*. **4231** pp. 73-78 (2000)
11. Bin, W., Lei, J. & Tian, Q. Study on computer-aided alignment method of Cassegrain system. *5th International Symposium On Advanced Optical Manufacturing And Testing Technologies: Large Mirrors And Telescopes*. **7654** pp. 29-34 (2010)
12. Thompson, K. Description of the third-order optical aberrations of near-circular pupil optical systems without symmetry. *Journal Of The Optical Society Of America A*. **22**, 1389-1401 (2005)
13. Fuerschbach, K., Rolland, J. & Thompson, K. Nodal aberration theory applied to freeform surfaces. *International Optical Design Conference*. pp. ITh2A-5 (2014)
14. Feng, S., Chen, Q., Gu, G., Tao, T., Zhang, L., Hu, Y., Yin, W. & Zuo, C. Fringe pattern analysis using deep learning. *Advanced Photonics*. **1**, 025001-025001 (2019)
15. Zhao, Z., Li, B., Lu, J., Kang, X. & Liu, T. One-shot phase retrieval method for interferometry using a hypercolumns convolutional neural network. *Optics Express*. **29**, 16406-16421 (2021)
16. Nishizaki, Y., Valdivia, M., Horisaki, R., Kitaguchi, K., Saito, M., Tanida, J. & Vera, E. Deep learning wavefront sensing. *Optics Express*. **27**, 240-251 (2019)
17. Zhang, L., Zhou, S., Li, J. & Yu, B. Deep neural network based calibration for freeform surface misalignments in general interferometer. *Optics Express*. **27**, 33709-33723 (2019)
18. Saha, S. Modern optical astronomy: technology and impact of interferometry. *Reviews Of Modern Physics*. **74**, 551 (2002)
19. Zhang, Z., Wang, H., Xu, F. & Jin, Y. Complex-valued convolutional neural network and its application in polarimetric SAR image classification. *IEEE Transactions On Geoscience And Remote Sensing*. **55**, 7177-7188 (2017)
20. Wang, R., Wang, Z., Chen, Y., Kang, H., Luo, F. & Liu, Y. Target recognition in SAR images using complex-valued network guided with sub-aperture decomposition. *Remote Sensing*. **15**, 4031 (2023)
21. Noll, R. Zernike polynomials and atmospheric turbulence. *Journal Of The Optical Society Of America*. **66**, 207-211 (1976)
22. Raissi, M., Perdikaris, P. & Karniadakis, G. Physics-informed neural networks: A deep learning framework for solving forward and inverse problems involving nonlinear partial differential equations. *Journal Of Computational Physics*. **378** pp. 686-707 (2019)
23. Zemax Optical Design Software [Online]. (Available: https://support.zemax.com/hc/en-us/categories/1500000770122-Tutorials-Applications,2024), [Accessed: 25 May 2024]